

The Thermodynamical Limit of the Lipkin-Meshkov-Glick Model

Pedro Ribeiro,¹ Julien Vidal,¹ and Rémy M osser¹

¹Laboratoire de Physique Théorique de la Matière Condensée, CNRS UMR 7600, Université Pierre et Marie Curie, 4 Place Jussieu, 75252 Paris Cedex 05, France

A method based on the analysis of the Majorana polynomial roots is introduced to compute the spectrum of the Lipkin-Meshkov-Glick model in the thermodynamical limit. A rich structure made of four qualitatively different regions is revealed in the parameter space whereas the ground state study only distinguishes between two phases.

PACS numbers: 05.30.-d, 21.60.Ev, 03.65.Sq

The Lipkin-Meshkov-Glick (LMG) model introduced in 1965 to describe shape phase transition in nuclei [1] has, since then, been proposed to describe many systems ranging from interacting spin systems [2] to Bose-Einstein condensates [3] or magnetic molecules such as Mn₁₂ acetate [4]. This ubiquity is due to its mapping onto a single-particle evolving in a double-well potential [5, 6] or onto an interacting two-levelboson system. More recently, this model has also been used to investigate the relationship between entanglement and quantum phase transitions [7, 8, 9, 10].

The LMG model is known to be exactly solvable [11, 12, 13]. However, getting the solution requires to solve Bethe-like equations, a task which, in the present context, is more costly than exact diagonalization. A complete description of the spectrum thus requires to develop alternative routes. Though the low-energy spectrum has been studied in details via different methods (variational [1], bosonization [9, 14], coherent states [15]), the richness of the full spectrum has been investigated only lately by means of numericaldiagonalizations [16, 17]. These latter studies suggest the existence of singular points in the density of states as well as a nontrivial level spacing distribution.

In this paper, we shed light on these issues by exactly computing the spectrum of the LMG model. The proposed method relies on the determination of the Majorana polynomial roots associated to the eigenstates of the Hamiltonian. This polynomial is built within a coherent state formalism which is well-suited to such a system. Within this framework, the spectrum is encoded in a linear differential equation which is solved in the thermodynamical limit. This allows us to exactly compute the density of states in the whole parameter range and to locate its singularities. Four distinct regions arise with qualitatively different properties. In particular, we find a parameter regime for which the density of states has no thermodynamical limit.

The LMG model describes a set of N spins $\frac{1}{2}$ mutually interacting through a X - Y -like Hamiltonian and coupled to an external transverse magnetic field h . This Hamiltonian H can thus be expressed in terms of the total spin operators $S_i = \sum_{i=1}^N \sigma_i$ where the σ_i 's are the Pauli

matrices:

$$H = \frac{1}{N} (xS_x^2 + yS_y^2 + hS_z) \quad (1)$$

In the following, we only consider the maximum spin sector $s = N/2$ with N even. Given the symmetry of the spectrum of H , we focus on the parameter range $h > 0$; $0.6 \leq h \leq x$. Note also that $H; S^2 = 0$ and $H; e^{i(S_z - s)} = 0$ (spin- $\frac{1}{2}$ symmetry). Denoting by $\{f_j\}_{j=0}^m$ the standard eigenbasis of $S^2; S_z$, this latter symmetry implies that odd and even states decouple. In the thermodynamical limit, both subspaces are isospectral so that we limit the following analysis to the sector m even for which one has exactly $(s+1)$ eigenstates.

In the spin coherent states basis [18], with normalized states $|j, i\rangle = e^{S_z - \frac{1}{2}s} |j, s\rangle$, any state $|j, i\rangle$ is represented by its Majorana polynomial [19] defined as

$$|\psi\rangle = h|j, i\rangle = \sum_{m=s}^s \frac{S^s}{(2s)!} \frac{(2s)!}{(s-m)!(m+s)!} h^{s-m} j^{m+s} |j, s\rangle \quad (2)$$

$$= C \sum_{k=1}^d (|j, k\rangle)$$

where $d = 2s$ is its degree.

The standard representation of the spin operators ($S_x = S_x - iS_y$) in the coherent states basis

$$S_+ = 2s \quad \theta^2 \quad ; \quad (3)$$

$$S_- = \theta \quad ; \quad (4)$$

$$S_z = s + \theta \quad ; \quad (5)$$

allows to map the Schrödinger equation $H|j, i\rangle = E|j, i\rangle$ onto the following linear differential equation [5, 20]

$$\frac{P_2(\theta)}{(2s)^2} \theta^2 + \frac{P_1(\theta)}{2s} \theta + P_0(\theta) \quad (\theta) = "(\theta); \quad (6)$$

where $" = E - s$ and

$$P_0(\theta) = \frac{1}{4s} \theta^2 (2s-1)(y-x) \quad x \quad y + h; \quad (7)$$

$$P_1(\theta) = \frac{2s-1}{2s} \theta^2 (x-y) \quad x \quad y + 2h; \quad (8)$$

$$P_2(\theta) = \frac{1}{2} \theta^2 (1^2 x^2 + 1^2 y^2); \quad (9)$$

Except for trivial values of the parameters, the degree of freedom for an eigenstate of H in the sector we considered is $d = 2s$. At this step, the spectrum could be analyzed by mapping Eq. (6) onto a Schrödinger equation describing a particle in an effective one-dimensional potential [5, 6]. Then, a semi-classical treatment would, in principle, allow one to obtain the density of states in the thermodynamical limit, as shown in Ref. [4] for the low-energy spectrum in the region $y = 0$; $x > 0$. Unfortunately, for arbitrary values of the parameters, the effective potential becomes tricky [6] and such an approach is therefore difficult to follow. Here, we propose an alternative route by first converting the linear second-order differential equation for (6) into a first-order differential equation for its logarithmic derivative. More precisely, the function G defined as

$$G(\zeta) = \frac{1}{2s} \theta \log(\zeta) = \frac{1}{2s} \sum_{k=1}^{2s} \frac{1}{\zeta^k}; \quad (10)$$

satisfies the following Riccati-like equation

$$P_2(\zeta) \frac{G^0(\zeta)}{2s} + G^2(\zeta) + P_1(\zeta)G(\zeta) + P_0(\zeta) = 0; \quad (11)$$

The density of states is then given by analyzing the poles of G , i.e., the roots of the Majorana polynomial. Indeed, the cornerstone of this study is that, for this model, the ζ 's are spread over two curves C_0 and C_1 in the complex plane which depend on the energy. In addition, the n -th excited state of H has $2n$ poles on C_1 and $2(s-n)$ on C_0 (thus defining both curves). This remarkable property stems from the oscillation theorem which indexes the excited states for a particle in the effective one-dimensional potential (discussed above) by the number of wavefunction nodes. To illustrate this repartition of the poles which is likely related to the integrability of the model [21], we display in Fig. 1 several typical states in the Majorana sphere representation [19]. This representation generalizes the celebrated Bloch sphere used for spin $\frac{1}{2}$ states and proceeds as follows. For a given polynomial with d roots, we first complement it with $(2s-d)$ roots at infinity in the complex plane. Next, the resulting set of $2s$ points is sent onto the unit sphere by an inverse stereographic map. For instance, within this mapping, the basis state $|jm\rangle$ is represented by $(s-m)$ points on one pole and $(s+m)$ points on the opposite pole.

The location of the poles of G explained above provides a straightforward relation between the normalized integrated density of states N [0;1] and the number of poles lying in C_1 . One indeed simply has

$$N(\eta) = \frac{n+1}{s+1} = \frac{1}{s+1} \sum_{\zeta \in C_1} \int_{\zeta}^{\infty} G(\zeta) d\zeta + 1; \quad (12)$$

where C_1 is a contour that surrounds C_1 and oriented such that $N \rightarrow 0$. In this equation, G is built from the n -th

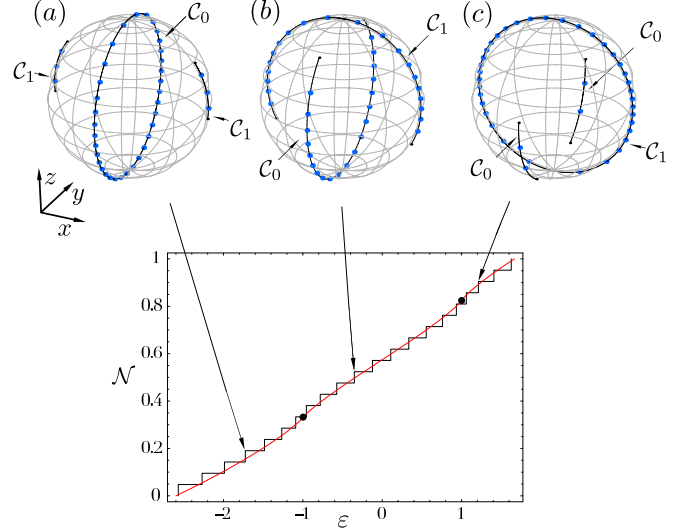


FIG. 1: Upper part: representation of the poles of G on the Majorana sphere (blue dots) for three typical eigenstates computed for $h = 1$; $x = 5$; $y = -3$ and $s = 20$ (zone III in Fig. 2). Black lines correspond to the G_0 branch cuts C_0 and C_1 .

Lower part: Numerical (black curve $s = 20$) versus analytical (red line $s = 1$) integrated density of states. Black dots indicates the singularity of the density of states $N_0^{III}(h)$ and $N_0^{III}(h)$ (Eqs. (18) and (21) respectively) in the thermodynamical limit.

excited state and the dependence of N with η is given via Eq. (11). Unfortunately, one cannot solve Eq. (11) exactly at finite s , which would give a complete explicit solution to our problem. However, one can easily solve it perturbatively in $1=s$.

Therefore, let us assume that G , and η , can be expanded in the following form

$$G = \sum_{i \in \mathbb{N}} \frac{G_i}{s^i}; \quad \eta = \sum_{i \in \mathbb{N}} \frac{\eta_i}{s^i}; \quad (13)$$

At leading order s^0 , Eq. (11) becomes a second-order polynomial equation for G_0 whose solutions simply read

$$G_0(\zeta) = \frac{\zeta^2(y-x) + x + y + 2h}{2P_2(\zeta)} \frac{P}{2Q(\zeta)}; \quad (14)$$

where

$$Q(\zeta) = (y-x)(h+\eta_0)^4 + 2h^2 + x^2y + \eta_0(x+y)^2 + (x-y)(h-\eta_0); \quad (15)$$

The four roots of Q are the branch points of G which define the limit of the curves C_0 and C_1 . A close analysis of these branch cuts, in the parameter space, then leads to the integrated density of states in the thermodynamical limit which reads

$$\lim_{s \rightarrow 1^-} N(\eta) = N_0(\eta_0) = \frac{1}{2i} \int_{C_1} G_0^+(\zeta) - G_0^-(\zeta) d\zeta; \quad (16)$$

This quantity can be expressed in terms of lengthy expressions involving elliptic integrals. We obtained these expressions in the whole parameter space and will give them explicitly in a forthcoming publication [22]. In the following, we only discuss qualitatively the various regions that must be distinguished, and analyze them by means of the density of states $\rho_0(\varepsilon_0) = \Theta(\varepsilon_0) N_0(\varepsilon_0)$.

But, first of all, let us remind the reader that if one only considers the properties of the ground state, which define the zero-temperature phase diagram, only two phases must be distinguished. For $h > \varepsilon_x$ (symmetric phase), the ground state is unique and $\lim_{s \rightarrow 1} h S_z = 1$ whereas for $h < \varepsilon_x$ (broken phase), the ground state is two-fold degenerate and $\lim_{s \rightarrow 1} h S_z = h = \varepsilon_x$. The quantum phase transition at $h = \varepsilon_x$ is second-order and characterized by mean-field critical exponents [2] and nontrivial finite-size scaling behavior [9, 23]. An important result of our study is that, when considering the full spectrum, four different zones arise instead of two. These regions, described below, are characterized by different singular behaviors of the density of states (see Fig. 2) as already noticed in a numerical study of the special case $\varepsilon_x = \varepsilon_y$ [16].

Zone I: $\varepsilon_y < \varepsilon_x < h$. In this sector, the density of states ρ_0 is a smooth function of $h \in [\varepsilon_0, h]$ as can be seen in Fig. 2. The distribution of Majorana polynomial roots for the eigenstates is similar to that displayed in Fig. 1(b). In the complex plane, C_0 and C_1 lie in the imaginary and real axes respectively.

Zone II: $\varepsilon_y < h < \varepsilon_x$. In this region, two distinct branches must be distinguished:

II(a): $\frac{h^2 + \varepsilon_x^2}{2\varepsilon_x} \leq \varepsilon_0 \leq h$. C_0 coincides with the whole imaginary axis while C_1 is made of two disconnected segments in the real axis as depicted in Fig. 1(a);

II(b): $h \leq \varepsilon_0 \leq h$. C_0 and C_1 are the same as in I.

These two branches of the density of states diverge at $\varepsilon_0 = h$ where the elliptic integrals involved in the expression of N_0 can be recasted in the simple following form

$$N_0^{II}(h) = 1 - \frac{2}{p \frac{x}{y}} A_h^+ \tan^{-1} \frac{A_h^+}{B_h^0} - A_h \tan^{-1} \frac{A_h}{B_h^+}; \quad (17)$$

with

$$A_h = h \frac{p}{x-y}; \quad (18)$$

$$B_h^0 = p \frac{h}{x} + p \frac{h}{y} + \frac{q}{(x-h)(h-y)}; \quad (19)$$

$$B_h = \left(\frac{p}{h-x} + \frac{p}{h-y} \right) + \frac{q}{(x-h)(h-y)}; \quad (20)$$

Zone III: $h < \varepsilon_y < \varepsilon_x$. In this zone, there are three different branches:

III(a): $\frac{h^2 + \varepsilon_x^2}{2\varepsilon_x} \leq \varepsilon_0 \leq h$. C_0 and C_1 are the same as in II(a);

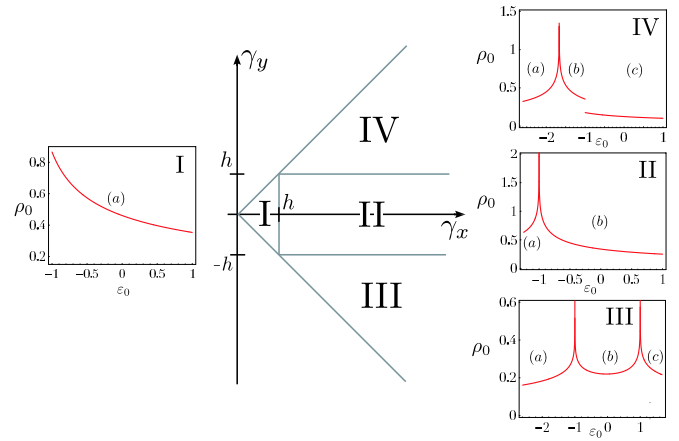


FIG. 2: Phase diagram in the $\varepsilon_x; \varepsilon_y$ plane at fixed $h > 0$ and typical density of states for $(\varepsilon_x; \varepsilon_y; h)$ equal to I: $(1=2; 1=3; 1)$, II: $(2; 1=2; 1)$, III: $(5; -3; 1)$, IV: $(5; 3; 1)$.

III(b): $h \leq \varepsilon_0 \leq h$. C_0 and C_1 are the same as in I;

III(c): $h \leq \varepsilon_0 \leq \frac{h^2 + \varepsilon_x^2}{2\varepsilon_x}$. C_0 is made of two disconnected segments in the imaginary axis while C_1 coincides with the whole real axis as depicted on the Majorana sphere in Fig 1(c).

In this zone, the density of states has two singularities at $\varepsilon_0 = h$. Their position in the spectrum is given by $N_0^{III}(h) = N_0^{II}(h)$ [see Eq. (18)] and

$$N_0^{III}(h) = \frac{2}{p \frac{x}{y}} A_h^+ \tan^{-1} \frac{A_h^+}{B_h^0} - A_h \tan^{-1} \frac{A_h}{B_h^+}; \quad (21)$$

For $\varepsilon_x = \varepsilon_y$, the density of states is symmetric with respect to $\varepsilon_0 = 0$, and the above expression gives the exact location, in the thermodynamical limit, of the so-called exceptional point observed in Ref. [16].

Zone IV: $h < \varepsilon_y < \varepsilon_x$. This part of the phase diagram is the most complex one. The density of states is, as in zone III, made of three different branches:

$$IV(a): \frac{h^2 + \varepsilon_x^2}{2\varepsilon_x} \leq \varepsilon_0 \leq \frac{h^2 + \varepsilon_y^2}{2\varepsilon_y};$$

$$IV(b): \frac{h^2 + \varepsilon_y^2}{2\varepsilon_y} \leq \varepsilon_0 \leq h;$$

$$IV(c): h \leq \varepsilon_0 \leq h.$$

However, the structure of the C_1 curve, in each case, is complex but C_0 remains simple so that the integral in Eq. (16) can still be computed and reveals two special points. The first one occurs at $\varepsilon_0 = \frac{h^2 + \varepsilon_x^2}{2\varepsilon_x}$ for which

$$N_0^{IV} \left(\frac{h^2 + \varepsilon_x^2}{2\varepsilon_x} \right) = 1 - \frac{1}{p \frac{x}{y}} \quad (22)$$

$$A_h^+ \tan^{-1} C_h - A_h \tan^{-1} C_h;$$

with

$$C_h = \frac{h \frac{p}{x-y} + \frac{3}{2} h^2}{\left(\frac{p}{x-y} \right) \left(\frac{p}{y} \right)}; \quad (23)$$

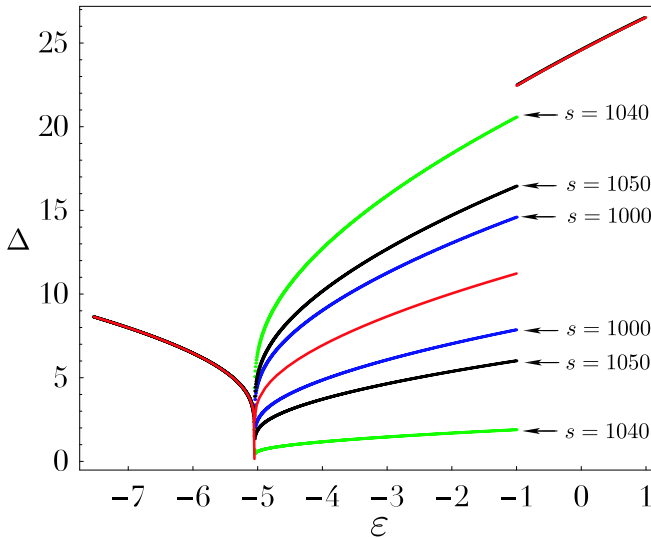


FIG. 3: Gap between two consecutive levels as a function of the energy in region IV for $x = 15$, $y = 10$ and $h = 1$. In the central region, the red line is the average gap in the thermodynamical limit (see text).

There, the density of states diverges as in zone II and III. The second one arises at $\epsilon_0 = -h$ where

$$N_0^{IV}(h) = 1 - \frac{h}{\pi \sqrt{xy}}; \quad (24)$$

but, at this energy, the density of states is discontinuous in the thermodynamical limit as can be seen in Fig. 2. We have confirmed this anomalous behavior numerically and observed an even more surprising result. Contrarily to all other regions, the density of states in region IV (b) computed for increasing s , does not converge towards the analytical result and, actually, does not converge at all. To understand this mismatch, let us consider the energy difference between two consecutive levels $\epsilon^{(i)} = E^{(i+1)} - E^{(i)}$ which, in the thermodynamical limit, converges towards $\epsilon_0(\epsilon_0) = 1 - \epsilon_0(\epsilon_0)$. In the region IV (b), $\epsilon^{(i)}$ spreads over two branches (+) and (-), depending on the parity of the i , which oscillate without converging when s increases, as can be seen in Fig. 3. In this case, the gap we compute, in the thermodynamical limit, is actually the average gap, namely $\epsilon_0(\epsilon_0) = \frac{1}{2}(\epsilon_0(+)) + \epsilon_0(-)(\epsilon_0)$.

Finally, note that for $h = 0$, the LMG model in this region coincides with the quantum asymmetric rotor model [24].

In conclusion, we would like to emphasize that the present approach can be extended to other similar models

with higher-order interactions where the mapping onto a particle in a one-dimensional potential fails. Further, one can go beyond the thermodynamical limit and extract the finite- s corrections which could be crucial for some observables [22].

We are grateful to C. A. Salgul, S. Dusuel, N. Gromov, J.-M. Maitland and P. Vieira for fruitful and stimulating discussions. PR was partially supported by FCT and EU FEDER through POCTI and POCI, namely via QuantLog POCI/MAT/55796/2004 Project of CLC-DM-IST, SQIG-IT and grant SFRH/BD/16182/2004/2ZB5.

- [1] H. J. Lipkin, N. M. Eshkov, and A. J. Glick, Nucl. Phys. 62, 188 (1965).
- [2] R. Botet and R. Jullien, Phys. Rev. B 28, 3955 (1983).
- [3] J. I. Cirac, M. Lewenstein, K. M. Mller, and P. Zoller, Phys. Rev. A 57, 1208 (1998).
- [4] D. A. Garanin, X. Martinez Hidalgo, and E. M. Chudnovsky, Phys. Rev. B 57, 13639 (1998).
- [5] A. V. Turbiner, Commun. Math. Phys. 118, 467 (1988).
- [6] V. V. Ulyanov and O. B. Zaslavskii, Phys. Rep. 216, 179 (1992).
- [7] J. Vidal, G. Palacios, and R. Mosseri, Phys. Rev. A 69, 022107 (2004).
- [8] J. I. Latorre, R. Orús, E. Rico, and J. Vidal, Phys. Rev. A 71, 064101 (2005).
- [9] S. Dusuel and J. Vidal, Phys. Rev. Lett. 93, 237204 (2004).
- [10] T. Barthel, S. Dusuel, and J. Vidal, Phys. Rev. Lett. 97, 220402 (2006).
- [11] F. Pan and J. P. Draayer, Phys. Lett. B 451, 1 (1999).
- [12] J. Links, H.-Q. Zhou, R. H. M. McKenzie, and M. D. Gould, J. Phys. A 36, R63 (2003).
- [13] G. Ortiz, R. Somma, J. Dukelsky, and S. Rombouts, Nucl. Phys. B 707, 421 (2005).
- [14] A. Dzhioev, Z. Aouissat, A. Storozhenko, A. Vodovotz, and J. Wambach, Phys. Rev. C 69, 014318 (2004).
- [15] A. Kuriyama et al, J. Phys. A 36, 10361 (2003).
- [16] W. D. Heiss, F. G. Scholz, and H. B. Geyer, J. Phys. A 38, 1843 (2005).
- [17] O. Castanos, R. Lopez-Pena, J. G. Hirsch, and E. Lopez-Moreno, Phys. Rev. B 74, 104118 (2006).
- [18] J. R. Klauder and B. S. Skagerstam, Coherent States (World Scientific, Singapore, 1985).
- [19] E. Majorana, Nuovo Cimento 9, 43 (1932).
- [20] J. Kurchan, P. Leboeuf, and M. Saraceno, Phys. Rev. A 40, 6800 (1989).
- [21] P. Leboeuf and A. Voros, J. Phys. A 23, 1765 (1990).
- [22] P. Ribeiro, J. Vidal, and R. Mosseri, in preparation.
- [23] F. Leyvraz and W. D. Heiss, Phys. Rev. Lett. 95, 050402 (2005).
- [24] G. W. King, J. Chem. Phys. 15, 820 (1947).